American Astronautical Society

American Institute of
Aeronautics and Astronautics

SUN HEADING ESTIMATION USING UNDERDETERMINED SET OF COARSE SUN SENSORS

Stephen A. O'Keefe and Hanspeter Schaub

AAS/AIAA Astrodynamics Specialists Conference

Hilton Head, South Carolina   August 11–15, 2013

SUN HEADING ESTIMATION USING UNDERDETERMINED SET OF COARSE SUN SENSORS

Stephen A. O'Keefe[*]and Hanspeter Schaub[†]

A comparison of two different methods to estimate the sun direction vector using an underdetermined set of cosine-type coarse sun sensors is presented. These methods are used in conjunction with a control law to reorient a spacecraft to a power positive orientation. Coarse sun sensors are commonly used to perform coarse attitude determination and accurately point a spacecraft's solar arrays at the Sun. These sensors are attractive due to their relative inexpensiveness, small size, and reduced power consumption. This paper presents two methods for accurately solving for the sun direction vector with decreased sensor requirements, the first is a simple weighted average method and the second leverages an extended Kalman filter approach. Both methods are combined with a control law and shown through numerical simulation to be capable of reorienting the spacecraft from any initially unknown attitude to a power positive state in a matter of minutes. While the EKF provides a more accurate sun heading estimate, the weighted average approach is simpler to implement and insensitive to common coarse sun sensor output calibration errors.

INTRODUCTION

Spacecraft commonly use a number of sun sensors to determine the sun direction vector in the body frame. High accuracy sun sensors often combine multiple measurements[1] or use charge-couple-devices (CCDs)[2] to determine the direction of the Sun. These digital sensors output a vector observation of the sun direction and two or more vector observations can be combined to deterministically solve for the true sun direction. Many methods exist for solving such a problem including TRIAD,[3] Davenport's Q-Method,[4] QUEST,[5] FOAM,[6] and OLAE.[7]

Alternatively, cosine-type coarse sun sensors (CSS) output a voltage relative to the input light and are attractive due to their inexpensiveness, small size, and minimal power consumption. These sensors are often used, in concert with other sensors,[8,9] during deployment to accurately point the spacecraft's solar arrays at the Sun to achieve power positiveness or to perform coarse attitude determination. Unfortunately, these cosine-type CSS output a scalar measurement, not a vector observation, and so deterministic methods that rely on multiple vector observation are not usable.

Instead, the sun direction vector must be determined through the use of geometric or statistical filtering algorithms. A spacecraft's attitude can generally be determined geometrically at any particular time if the Sun is simultaneously in the field of view of at least three cosine-type sensors; a more reliable estimate can be achieved if continuous 4π steradian coverage can be achieved with four sensors. Statistical filtering algorithms provide an estimate of the spacecraft's attitude based on

[*]Graduate Research Assistant, Aerospace Engineering Sciences, University of Colorado, Boulder, CO
[†]Professor, H. Joseph Smead Fellow, Aerospace Engineering Sciences, University of Colorado, Boulder, CO

a collection of measurements over time. In particular, sequential filtering algorithms process measurements as soon as they are received and are commonly derived from the Kalman filter[10] which produces a statistically optimal estimate of the system. The Kalman filter assumes a linear dynamical system and many variants have been developed for nonlinear systems, the most popular variant is the extended Kalman filter[11] which linearizes the nonlinear system about the current estimate.

Because CSS are relatively inexpensive, it is not uncommon for spacecraft to have a multitude of sensors placed around the exterior to achieve the coverage required for determining the sun direction geometrically. The addition of so many sensors to the spacecraft is not without hazards. Care must be taken so that the fields of view of the CSS are not blocked by other instrumentation and the amount of internal cabling required can become prohibitive. The placement of these sensors is generally an iterative process based on experience and prior designs but can be optimized through various methods.[12]

If, however, it is unfeasible to use a large number of CSS or additional instrumentation, due to budgetary, power, or space constraints, and the spacecraft must still accurately orient its solar arrays at the Sun following deployment, an alternative method is proposed. The sun direction is not needed initially to high precision in order for the spacecraft to maneuver to a sun pointing orientation. In fact, a full three degree of freedom description is not needed as rotation about the solar array normal vector will not negatively impact power generation. In this situation low fidelity estimates of the sun direction are enough for a control law to begin reorienting the spacecraft using reaction wheels or thrusters. Therefore, fewer sensors are needed in regions far from the desired pointing vector and the total number of sensors required can be reduced. Once the spacecraft begins to reorient, more sensors oriented along the desired alignment axis help to refine the estimate of the sun direction vector and accurately point the spacecraft's solar arrays at the Sun. While the location of the Sun cannot be uniquely determined geometrically at each time step in the underdetermined case, the time histories of measurements from several CSS can be combined in an estimation filter to determine the sun direction vector. Once the spacecraft is pointing at the Sun and generating power, more accurate measurement sensors, such as star trackers, can be turned on to determine the spacecraft's absolute attitude.

This paper examines using CSS in an underdetermined configuration, both solely and in concert with a rate gyroscope, to orient a spacecraft's solar arrays at the Sun following deployment to determine how well low cost sensors can be used to maintain high performance. A comparison is made between a simple weighted average approach for determining the sun direction vector at a given time and an extended Kalman filter approach which incorporates time histories of measurements into the estimate. First, a description of the sensors and the spacecraft configuration used are presented. A basic weighted average method of determining the sun direction unit vector is detailed followed by an extended Kalman filter (EKF) formulation. Finally, numerical simulation results demonstrating the performance of each approach are presented.

COARSE SUN SENSOR CONFIGURATION

The cosine-type CSS used in this study are composed of photodiodes with a glass cover for filtering out undesired wavelengths and optionally baffles for restricting the field of view. The output voltage of the sensor is assumed to be given by[13]

$$V = V_0 \left({}^{\mathcal{B}}\hat{\boldsymbol{n}} \cdot {}^{\mathcal{B}}\hat{\boldsymbol{s}} \right) \tag{1}$$

(a) Schematic of spacecraft.

(b) Coarse sun sensor coverage map.
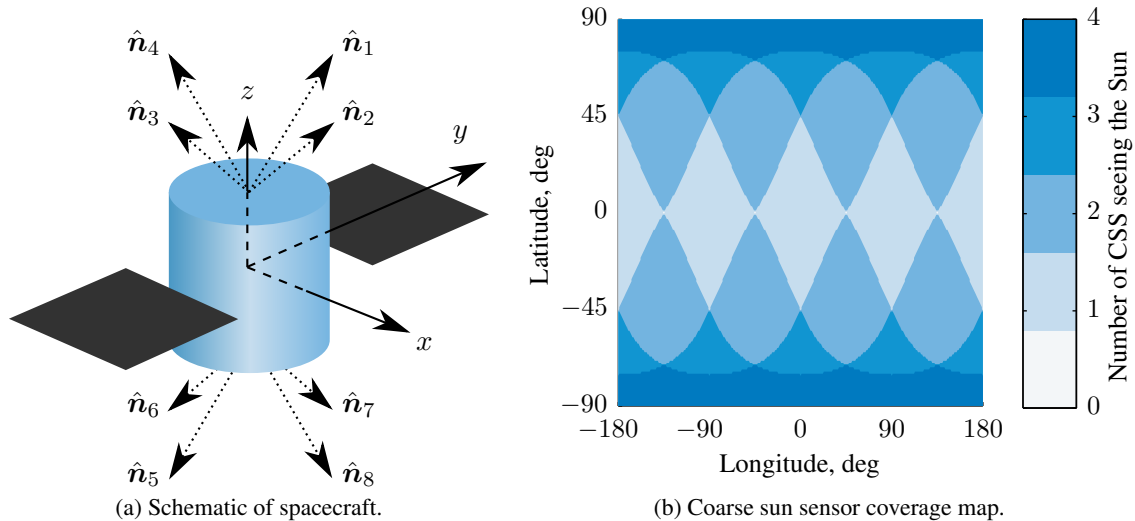
Figure 1: Illustration of spacecraft with CSS unit vectors $\hat{\boldsymbol{n}}_i$ for a dual pyramid configuration and the associated CSS coverage map.

where $\hat{\boldsymbol{n}}$ is the unit normal of the CSS, $^{\mathcal{B}}\hat{\boldsymbol{s}}$ contains the body frame $\mathcal{B}$ components of the unit direction vector from the spacecraft to the Sun, and V_0 is a scaling factor.

The spacecraft used for this study is assumed to be equipped with eight cosine-type CSS in a dual pyramid configuration. Four sensors with $120 \deg$ fields of view are arranged on the $+z$ and $-z$ faces of the spacecraft oriented $90 \deg$ apart and angled $45 \deg$ from the body z axis. An illustration of this configuration is shown in Figure 1a.

Figure 1b shows the number of CSS to which the Sun is visible for any relation of the Sun with respect to the spacecraft. This figure takes into account that the fields of view of the CSS are clipped at the local-horizontal plane by the spacecraft structure and solar panel arrays and thus the CSS cannot see the Sun when it is below the local (x, y) plane. As can be seen, multiple sensor coverage is provided along, $+z$, and opposite, $-z$, the solar array normal direction with minimal coverage along the equator of the spacecraft. This configuration leaves the sides of the spacecraft clear for scientific instrumentation and seeks to minimize both the CSS obstruction due to the solar arrays and the amount of internal cabling necessary for the sensors. For this study it is assumed if the solar array normal vector is within $30 \deg$ of the sun direction vector the spacecraft is in a power positive state, generating sufficient power to operate all instrumentation and recharge batteries.

SUN HEADING ESTIMATION

Because multiple sensor coverage is not available everywhere, the sun direction cannot be uniquely determined geometrically in areas of minimal sensor coverage. A simple method for calculating the sun direction vector in the body frame that is capable of giving an estimate even when only one sensor sees the sun involves taking a weighted average of all CSS output. A more robust method involves using a time history of measurements and dynamical equations for the system in an extended Kalman filter.
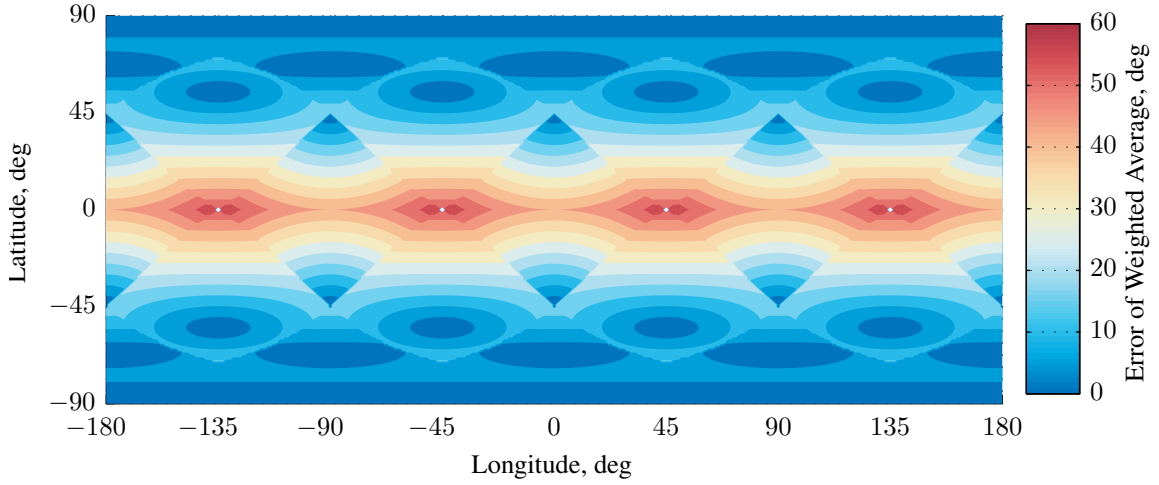
Figure 2: Weighted average method error map for any relation of the Sun with respect to the spacecraft.

Weighted Average Method

A simple method for determining the sun direction unit vector involves taking a weighted average of all the CSS capable of seeing the Sun using the equation

$$
{}^{\mathcal{B}}\tilde{\hat{s}} = \frac{\sum\limits_{i=1}^{N} V_i {}^{\mathcal{B}}\hat{n}_i}{\|\sum\limits_{i=1}^{N} V_i {}^{\mathcal{B}}\hat{n}_i\|} \tag{2}
$$

where N is the total number of sensors and V_i is the magnitude of the output of the ith sensor. The matrix ${}^{\mathcal{B}}\tilde{\hat{s}}$ contains the body frame $\mathcal{B}$ vector components of the best estimate of the sun heading vector $\hat{s}$. For the spacecraft configuration examined in this paper, there are regions where only one of the CSS senses the sun and the weighted average estimate is expected to suffer. This is verified in Figure 2, which shows the error map of the weighted average map. As can be seen, there is a large band near the equator of the spacecraft in which the error is greater than 30 deg. If the Sun is within this region, it will result in a large estimation error, but even an approximate sun heading estimate provides enough knowledge for the control to apply the appropriate rotation rate. The coverage at the poles is more important. The desired attitude of the spacecraft requires the sun direction vector be aligned with the z axis, and within 19 deg of this axis the error remains less than 10 deg. Thus, the control becomes more precise near the goal orientation.

This weighted average method is attractive as it is computationally simple, provides an error measure when only one sensor is seeing the Sun, and is capable of estimating the sun direction vector to within a few degrees using the configuration described here. Further, this method is insensitive to CSS calibration error as long as the calibration error is common across all sensors. An example of a common error would be if the flux seen by the sensors in space is different from the value used for calibration. This is seen by substituting Equation (1) into Equation (2); if the value of V_0 is scaled the same for all the sensors this factor will fall out of Equation (2).

Extended Kalman Filter Method

A common attitude estimation problem involves propagating the state dynamics and correcting that estimate using a direct measurement of the body's attitude. Thus, instead of solving the geometry of the CSS measurement values at any instant in time, a time history of sensor output can be used to correct an estimate of the sun vector being propagated. As noted previously, if the true sun vector lies in a region where only single sensor coverage exists the estimate can be significantly in error. An EKF approach overcomes these regions of unobservability through the accumulation of multiple measurements over time. The following section describes the application of a continuous-discrete extended Kalman Filter to the problem of estimating the sun direction unit vector in the spacecraft body frame. At first, it is assumed that the angular velocity of the spacecraft $\boldsymbol{\omega}$ is determined via a rate gyroscope.

The continuous-time state dynamics of the system can be represented as

$$\dot{\boldsymbol{x}} = \boldsymbol{f}(\boldsymbol{x}, \boldsymbol{u}, t) + \boldsymbol{g}(\boldsymbol{x}, \boldsymbol{\eta}, t) \tag{3}$$

where $\boldsymbol{f}$ represents the system dynamics, $\boldsymbol{g}$ is a process noise function, the state vector $\boldsymbol{x} = \begin{bmatrix} {}^{\mathcal{B}}\hat{\boldsymbol{s}} \end{bmatrix}$ is composed of the sun direction unit vector in the spacecraft body frame, and $\boldsymbol{\eta} \sim N(0, \boldsymbol{Q})$ represents an unbiased random noise vector. The time derivative of the sun direction unit vector is found by solving

$$\frac{{}^{\mathcal{N}}\mathrm{d}}{\mathrm{d}t}\left({}^{\mathcal{B}}\hat{\boldsymbol{s}}\right) = \frac{{}^{\mathcal{B}}\mathrm{d}}{\mathrm{d}t}\left({}^{\mathcal{B}}\hat{\boldsymbol{s}}\right) + {}^{\mathcal{B}}\boldsymbol{\omega} \times {}^{\mathcal{B}}\hat{\boldsymbol{s}} \tag{4}$$

assuming that for the time scales of interest the inertial sun vector can be assumed to be constant. Thus,

$$\boldsymbol{f}(\boldsymbol{x}, \boldsymbol{u}, t) = {}^{\mathcal{B}}\hat{\boldsymbol{s}} \times {}^{\mathcal{B}}\boldsymbol{\omega} \tag{5}$$

$$\boldsymbol{g}(\boldsymbol{x}, \boldsymbol{\eta}, t) = \boldsymbol{\eta}. \tag{6}$$

The continuous-time covariance propagation between measurements is given by the continuous-time Lyapunov differential equation[14]

$$\dot{\boldsymbol{P}} = \boldsymbol{F}\boldsymbol{P} + \boldsymbol{P}\boldsymbol{F}^T + \boldsymbol{G}\boldsymbol{Q}\boldsymbol{G}^T \tag{7}$$

where

$$\boldsymbol{F} \equiv \left.\frac{\partial \boldsymbol{f}}{\partial \boldsymbol{x}}\right|_{\hat{\boldsymbol{x}}} = -\left[{}^{\mathcal{B}}\boldsymbol{\omega}\right]_{\times} \qquad \boldsymbol{G} \equiv \left.\frac{\partial \boldsymbol{g}}{\partial \boldsymbol{\eta}}\right|_{\hat{\boldsymbol{x}}} = [I] \tag{8}$$

and $[\cdot]_{\times}$ represents the skew-symmetric cross product matrix given by

$$[\boldsymbol{\sigma}]_{\times} = \begin{bmatrix} 0 & -\sigma_3 & \sigma_2 \\ \sigma_3 & 0 & -\sigma_1 \\ -\sigma_2 & \sigma_1 & 0 \end{bmatrix}.$$

Assuming the gain V_0 in Equation (1) is calibrated such that the CSS return a value of 1 when aimed directly at the Sun, the coarse sun sensor measurements can be written as

$$\boldsymbol{h}(\boldsymbol{x}_k) = {}^{\mathcal{B}}\hat{\boldsymbol{n}}_i \cdot {}^{\mathcal{B}}\hat{\boldsymbol{s}} + {}^{\mathcal{B}}\boldsymbol{\eta}_{css} \tag{9}$$

where ${}^{\mathcal{B}}\boldsymbol{\eta}_{css}$ is an unbiased random noise vector with covariance $\boldsymbol{R}$. The discrete-time measurements from the ith coarse sun sensors

$$\tilde{\boldsymbol{y}}_{i_k} = V_i \tag{10}$$

can be incorporated into the state estimates using the extended Kalman filter with state updates given by

$$\bar{x}_k^+ = \bar{x}_k^- + K_k \left[\tilde{y}_k - h(\bar{x}_k^-) \right] \tag{11}$$

$$P_k^+ = \left[I - K_k H_k(\bar{x}_k^-) \right] P_k^- \left[I - K_k H_k(\bar{x}_k^-) \right]^T + K_k R_k K_k^T \tag{12}$$

where $\bar{x}_k^-$ is the propagated state estimate and $\bar{x}_k^+$ is the measurement corrected state estimate at time t_k, and P_k^- is the propagated covariance estimate and P_k^+ is the measurement corrected covariance estimate. The Kalman gain matrix K_k is given by

$$K_k = P_k^- H_k^T(\bar{x}_k^-) \left[H_k(\bar{x}_k^-) P_k^- H_k^T(\bar{x}_k^-) + R_k \right]^{-1} \tag{13}$$

where

$$H_k(\bar{x}_k^-) \equiv \left. \frac{\partial h}{\partial x} \right|_{\bar{x}_k^-} = \left[\hat{n}_i^T . \right] \tag{14}$$

This EKF method is attractive as it uses a time history of measurements to improve its estimate instead of using only measurements from a single point in time. In addition, its predictor corrector formulation allows it to predict when a sensor should see the Sun allowing it to use information from all of the CSS not just those that are currently outputting a voltage. Unfortunately, the EKF method is not robust to significant CSS calibration error like the weighted average method. In practice, a batch analysis of on orbit data is required to account for any large calibration errors.

Angular Rate Estimate

The control used to reorient the spacecraft to a power positive state requires a measure of the spacecraft's angular velocity in order to arrest any rates. In addition, while the weighted average method does not incorporate the spacecraft's angular velocity, the EKF method does require an estimate of the vehicle's rates in order to propagate the system dynamics. Nominally the angular velocity of the spacecraft is provided by a rate gyroscope, usually embedded within an inertial measurement unit. However, in a power critical situation it may be necessary to turn off the inertial measurement unit. For this situation, a simple estimate of the vehicle's angular velocity vector is developed using the two most recent estimates of the sun direction unit vector.

By taking the cross product of the current and previous estimates of the sun direction vector, an estimate of the direction of the body angular velocity vector $\bar{\omega}$ can be determined. This is then be scaled by the angle between the two vectors and divided by the time since the previous sun direction vector estimate to provide an estimate of the body angular velocity vector.

$$\bar{\omega}_k = \frac{{}^{\mathcal{B}}\hat{\bar{s}}_k \times {}^{\mathcal{B}}\hat{\bar{s}}_{k-1}}{\left\| {}^{\mathcal{B}}\hat{\bar{s}}_k \times {}^{\mathcal{B}}\hat{\bar{s}}_{k-1} \right\|} \frac{\cos^{-1}\left({}^{\mathcal{B}}\hat{\bar{s}}_k \cdot {}^{\mathcal{B}}\hat{\bar{s}}_{k-1} \right)}{\Delta t}. \tag{15}$$

Here ${}^{\mathcal{B}}\hat{\bar{s}}_k$ is the best estimate of the sun direction unit vector in the body frame at time t_k and Δt is the time since the last update. Note that with this rate estimate it is not possible to estimate the full three-dimensional ω vector as rates about ${}^{\mathcal{B}}\hat{s}$ are not observable. However, for the purpose of coarse sun pointing this is not an issue, as such rotations about the sun direction vector will not impact the solar panel incidence angle or the associated electrical power generation.

Results, shown later, show that this method provides an estimate adequate to achieve a power positive orientation. Because the estimate of the spacecraft's angular velocity vector is found through differentiation it is expected the amount of noise in the estimate will increase. To counteract this, the estimate is conservatively bounded about each axis and run through a first order low pass filter. The numerical simulation shown next assumes maximum tip off rates of 2.0 deg/sec about each axis so the bound on the angular rate estimate about each axis is set at 10 deg/sec.

NUMERICAL SIMULATION

An initially uncontrolled tumbling spacecraft is simulated to demonstrate the performance of both the weighted average method and the EKF method in estimating the sun heading and orienting the spacecraft in a power positive attitude. The spacecraft is modeled in a $400\,\mathrm{km}$ altitude circular orbit with an inclination of $45\,\mathrm{deg}$ starting on 2013 June 1, 00:00 UTC. For this orbit the spacecraft has a period of approximately 92.5 minutes and spends approximately 56.5 minutes in view of the Sun per orbit. Ephemeris for the Earth and Sun are calculated using the NASA Navigation and Ancillary Information Facility (NAIF) SPICE toolkit.[15]

Spacecraft parameters

The spacecraft is assumed to have a diagonal inertia matrix

$$[I] = \begin{bmatrix} 10.5 & 0 & 0 \\ 0 & 8 & 0 \\ 0 & 0 & 6.75 \end{bmatrix} \mathrm{kg\,m^2}.$$

and four reaction wheels with alignment axes given by

$$[G_s] = \begin{bmatrix} 0 & 0 & \cos(45°) & -\cos(45°) \\ \cos(45°) & \sin(45°) & -\sin(45°) & -\sin(45°) \\ \sin(45°) & -\cos(45°) & 0 & 0 \end{bmatrix}.$$

Each reaction wheel is assumed to have a spin-axis inertia of $J_s = 0.001\,\mathrm{kgm^2}$ and a maximum torque of $30\,\mathrm{mNm}$.

The spacecraft's initial attitude is uniformly distributed amongst all possible attitudes and its initial angular velocity is uniformly distributed about all three axes with a maximum value of $2.0\,\mathrm{deg/sec}$. Angular rate measurements are simulated at $10.0\,\mathrm{Hz}$ assuming a Gaussian distributed constant bias with a standard deviation of $1\,\mathrm{deg/hr}$ and white Gaussian noise with a standard deviation of $0.01\,\mathrm{deg/sec}$.

Course Sun Sensors

CSS measurements are updated at $10\,\mathrm{Hz}$ and are modeled with both internal and external error sources. Internal errors are modeled through the application of warping and degradation of the measurement and external errors are simulated using an Earth albedo model.

Warping is applied to the CSS measurements as shown in Figure 3 to represent an incorrect calibration. The warping represents a flattened peak response commonly seen on commercially available photodiodes and is applied through

$$V = V \left(1 + \frac{1}{2}\beta^2 - 0.65\beta^4\right) \tag{16}$$
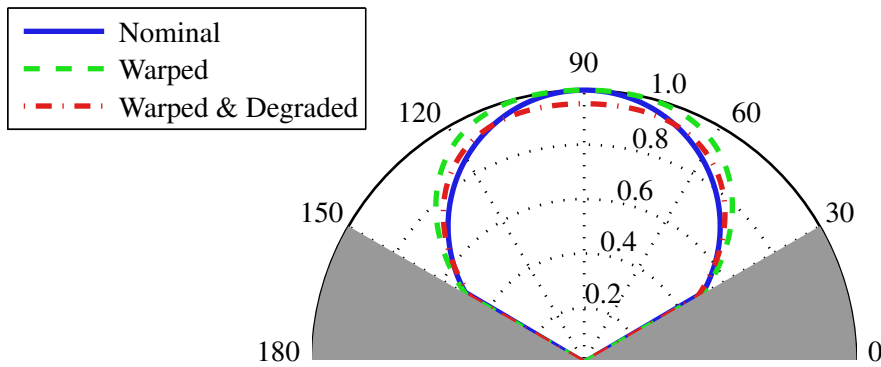
Figure 3: Illustration of CSS field of view and applied degradations.

where V is the output of the CSS and $\beta = \sin\left(\cos^{-1} V\right)$. Measurement magnitudes are also reduced uniformly up to 5 percent at every time step to simulate possible degradation over the lifetime of the sensor.

The cosine-type CSS used here are are sensitive to any light and on orbit the most significant light source other than direct sunlight is light from the Sun diffusely reflected by the Earth. Solar radiation that is absorbed by the Earth and later radiated at infrared wavelengths is easily filtered through mechanical means and the energy due to specular reflectance is generally small and ignored.[16] Assuming a Lambertian cosine law the output of the ith CSS due to the diffuse reflectance of the Earth V_{α_i} can be modeled as[8]

$$V_{\alpha_i} = \frac{V_{0_i}}{\pi} \int_{\boldsymbol{A}} \frac{\alpha}{\|\boldsymbol{r}_{AB}\|^2} \left(\hat{\boldsymbol{n}}_A \cdot \hat{\boldsymbol{s}}_E\right) \left(\hat{\boldsymbol{n}}_A \cdot \hat{\boldsymbol{r}}_{AB}\right) \left(\hat{\boldsymbol{r}}_{AB} \cdot \hat{\boldsymbol{n}}_i\right) dA \tag{17}$$

where $\boldsymbol{A}$ is the surface of the Earth visible to the spacecraft, $\left(\hat{\boldsymbol{n}}_A \cdot \hat{\boldsymbol{r}}_{AB}\right) > 0$ and $\left(\hat{\boldsymbol{r}}_{AB} \cdot \hat{\boldsymbol{n}}_i\right) \geq \cos\Delta$, that is also illuminated, $\left(\hat{\boldsymbol{n}}_A \cdot \hat{\boldsymbol{s}}_E\right) > 0$; $\hat{\boldsymbol{n}}_A$ is the unit normal of an incremental area on the surface of the Earth; $\hat{\boldsymbol{s}}_E$ is the unit direction vector from the Earth to the Sun; $\hat{\boldsymbol{r}}_{AB}$ is a vector from an incremental area on the surface of the Earth to the body of the spacecraft; and α is the albedo constant of the incremental area.

The albedo constant for the Earth is taken from the NASA Total Ozone Mapping Spectrometer mission data. The data used in this effort were acquired as part of the activities of NASA's Science Mission Directorate, and are archived and distributed by the Goddard Earth Sciences (GES) Data and Information Services Center (DISC). Daily measurements on a $5\deg \times 5\deg$ latitude longitude grid from 2000 to 2005 were used to generate mean and standard deviations for the reflectivity of Earth. These values are shown, with global coastlines superimposed for reference, in Figure 4.

To illustrate the significance of this error source the simulated output of the CSS, calculated using Equation (9) combined with Equation (17), for the nominal orbit discussed here is shown in Figure 5a. For comparison a similar polar orbit with a $90\deg$ inclination is shown in Figure 5b. As can be seen the CSS output due to albedo has a value approximately 25% of the output due to direct sunlight for an orbit inclined to $45\deg$. For a near polar orbit the CSS output due to albedo is predicted to be approximately 50% of the output due to direct sunlight.
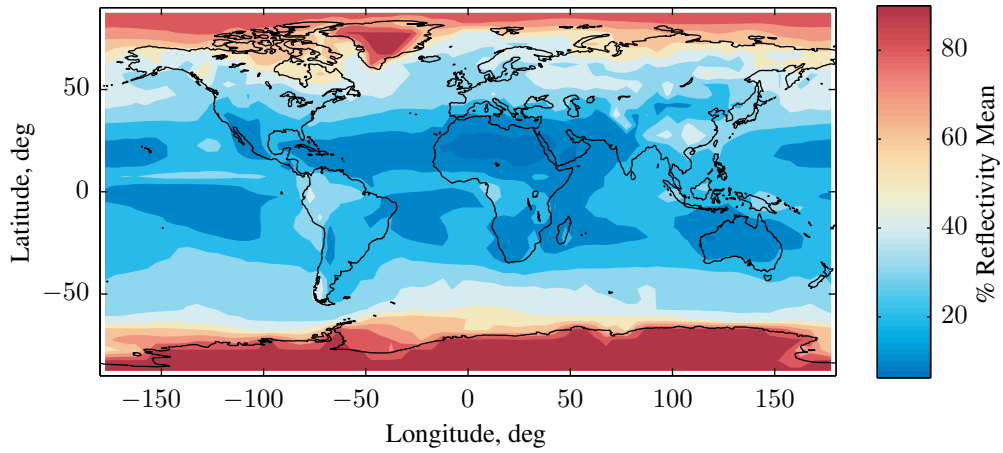
(a) Mean reflectivity.
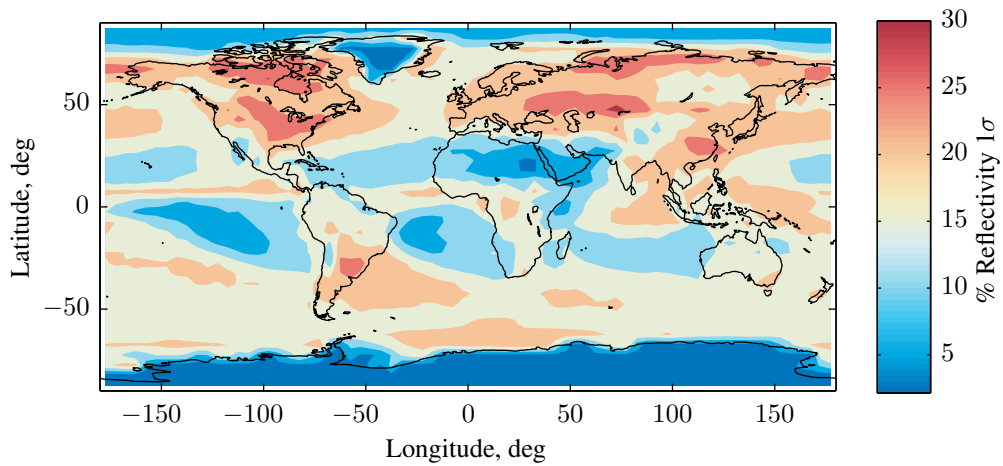
(b) Standard deviation of reflectivity.

Figure 4: Mean and standard deviation of the reflectivity of Earth as measured by TOMS mission between 2000 and 2005 used in numerical simulations.
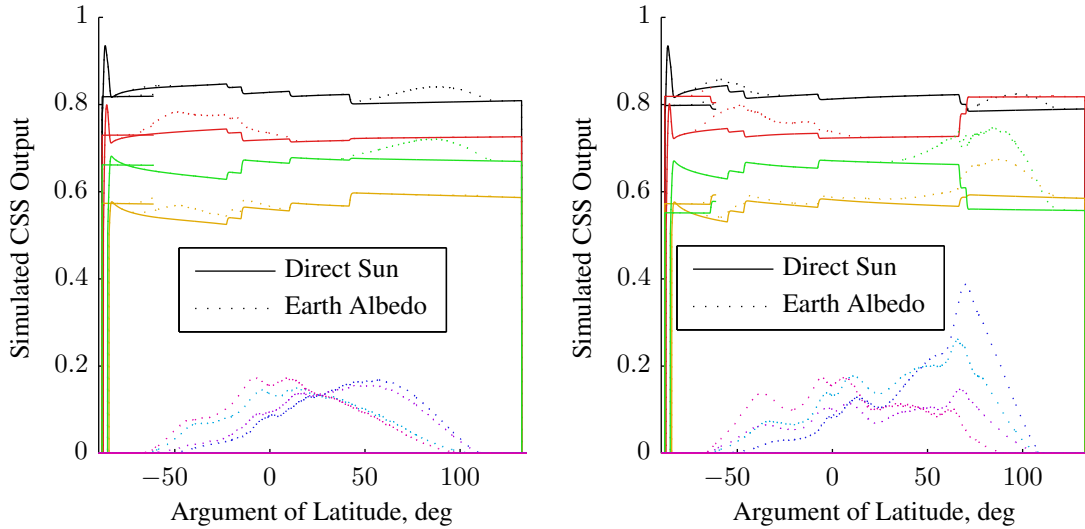
(a) Simulated CSS output for an orbit with $i = 45 \deg$.   (b) Simulated CSS output for an orbit with $i = 90 \deg$.

Figure 5: Simulated CSS output for 400 km circular orbit with varying inclinations demonstrating the significant impact of Earth's albedo. Output is shown for eight sensors arranged in a dual pyramid formation and the output due to albedo has been superimposed on top of the output due to direct sunlight.

Controller

A nonlinear three-axis attitude control is used in the numerical simulation to reorient the space-craft using redundant reaction wheels.[17] This control law was designed with detumbling and continuous autonomous momentum dumping in mind, and its goal is to orient the spacecraft body frame $\mathcal{B}$ with a reference frame $\mathcal{R}$ where the attitude error between the body and reference frames is described using the MRP set $\boldsymbol{\sigma}_{\mathcal{BR}}$. The reference attitude is assumed time-varying so the spacecraft must track the angular velocity of the reference frame $\boldsymbol{\omega}_r$. The control law is given by

$$
\begin{aligned}
[G_s]\, \boldsymbol{u}_s = & - [I]\left(\dot{\boldsymbol{\omega}}_r - [\boldsymbol{\omega}]_\times \boldsymbol{\omega}_r\right) + K\boldsymbol{\sigma}_{\mathcal{BR}} + [P]\,\delta\boldsymbol{\omega} + [P]\,[K_I]\,\boldsymbol{z} \\
& - \left([\boldsymbol{\omega}_r]_\times - [[K_I]\,\boldsymbol{z}]_\times\right)\left([I]\,\boldsymbol{\omega} + [G_s]\,\boldsymbol{h}_s\right) + \boldsymbol{L}
\end{aligned}
\tag{18}
$$

where $\delta\boldsymbol{\omega} = \boldsymbol{\omega} - \boldsymbol{\omega}_r$, K is a scalar gain, $[K_I]$ is a gain matrix, z is the integral term, and $[P]$ is a positive definite gain matrix.

The control is proven to be asymptotically stabilizing and guarantees if $\boldsymbol{\sigma}$ converges to zero so will $\delta\boldsymbol{\omega}$. For further discussion of this control law and its development the reader is referred to Reference 17. For this numerical simulation the control gains specified in Table 1 are used and $\boldsymbol{\omega}_r = \dot{\boldsymbol{\omega}}_r = \begin{bmatrix} 0 & 0 & 0 \end{bmatrix}^T$. The control is implemented with a deadband of $15 \deg$; if the sun direction vector falls within $15 \deg$ of the solar array unit vector the control is turned off.

Of importance to the implementation of this control law is the quantity $\boldsymbol{\sigma}_{\mathcal{BR}}$. The sun vector estimation algorithm computes a value for the sun direction unit vector in the body frame, not an attitude error. An error MRP is formed by finding the principal rotation vector necessary to rotate the sun direction vector ${}^{\mathcal{B}}\hat{s}$ to align with the solar array unit vector $\hat{c}$ expressed in the body frame.

Table 1: Control gains used for numerical simulation

$[K]$	$[P]$	$[K_I]$	c
$0.148\boldsymbol{I}_{3\times3}$ Nm	$0.9\boldsymbol{I}_{3\times3}$ Nms	$0.0001\boldsymbol{I}_{3\times3}$ N^{-1}s^{-2}	0.005 s^{-1}
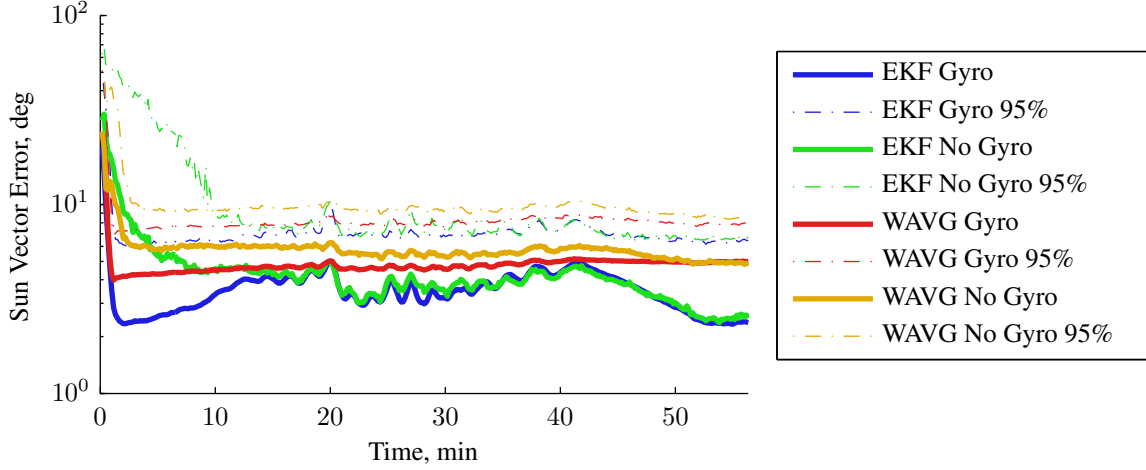
Figure 6: Statistics from 1000 case Monte Carlo analysis detailing the angular difference between the true sun direction and the estimate found using both the EKF and weighted average (WAVG) methods with and without rate gyro measurements.

This vector is then used in the definition of the MRP vector

$$\boldsymbol{\sigma} = \hat{\boldsymbol{e}} \tan\left(\frac{\Phi}{4}\right) \tag{19}$$

to create an error MRP. The equation for the error MRP is thus given by

$$\boldsymbol{\sigma}_{\mathcal{BR}} = \frac{{}^{\mathcal{B}}\hat{\boldsymbol{s}} \times {}^{\mathcal{B}}\hat{\boldsymbol{c}}}{\|{}^{\mathcal{B}}\hat{\boldsymbol{s}} \times {}^{\mathcal{B}}\hat{\boldsymbol{c}}\|} \tan\left(\frac{1}{4}\cos^{-1}\left({}^{\mathcal{B}}\hat{\boldsymbol{c}} \cdot {}^{\mathcal{B}}\hat{\boldsymbol{s}}\right)\right). \tag{20}$$

Equation (20) can result in a singularity when the denominator ${}^{\mathcal{B}}\hat{\boldsymbol{s}} \times {}^{\mathcal{B}}\hat{\boldsymbol{c}}$ approaches zero, or the solar array normal approaches alignment with the sun direction vector. However, as the value of the denominator goes to zero, so will the quantity ${}^{\mathcal{B}}\hat{\boldsymbol{c}} \cdot {}^{\mathcal{B}}\hat{\boldsymbol{s}}$. By simply setting the control to zero when the quantity ${}^{\mathcal{B}}\hat{\boldsymbol{c}} \cdot {}^{\mathcal{B}}\hat{\boldsymbol{s}}$ falls below a threshold, or control deadband, this issue is avoided.

Results

The resulting sun vector direction vector errors for a 1000 case Monte Carlo analysis are shown in Figure 6. Both the weighted average, denoted WAVG, and the EKF methods are simulated twice, once with angular velocity measurements from a rate gyroscope and once without. The total vehicle angular velocity is shown in Figure 7a and the errors in the estimate of the vehicle angular velocity are shown in Figure 7b. In all plots both the mean and 95th percentile values are shown.

Both the weighted average method and EKF methods successfully reorient the spacecraft, aligning the solar array unit normal with the sun direction vector. As expected, and as can be seen in
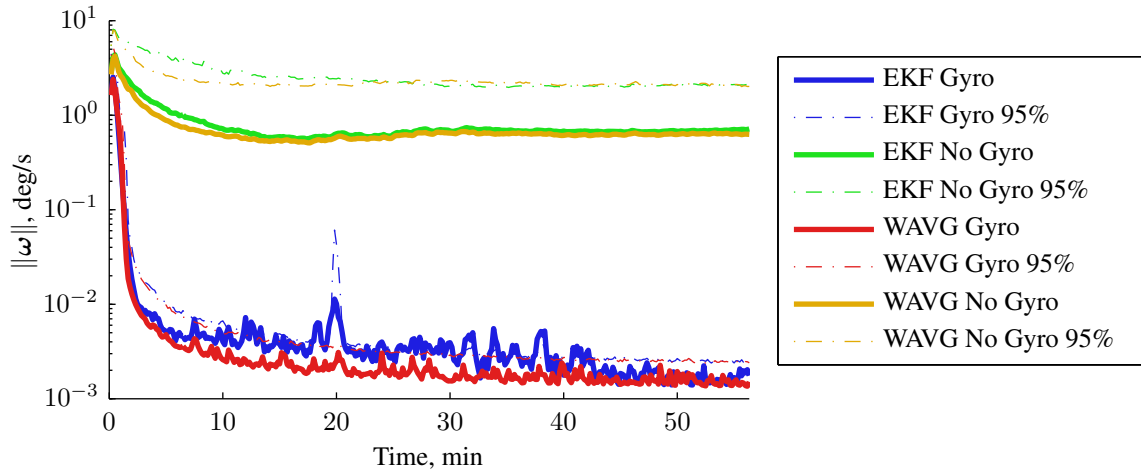
(a) Spacecraft angular velocity.
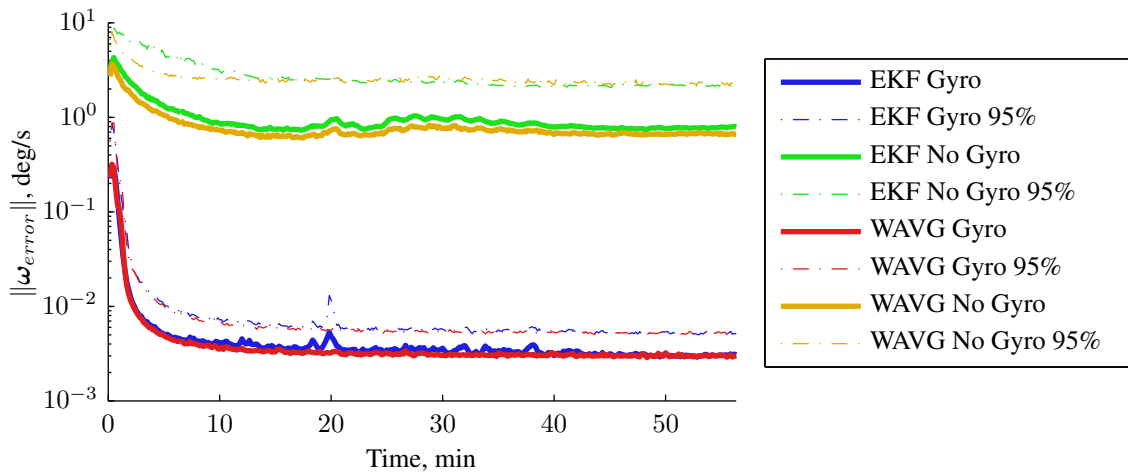
(b) Spacecraft angular velocity knowledge error.

Figure 7: Statistics from 1000 case Monte Carlo analysis for cases controlled by the EKF and weighted average (WAVG) methods with and without rate gyro measurements.
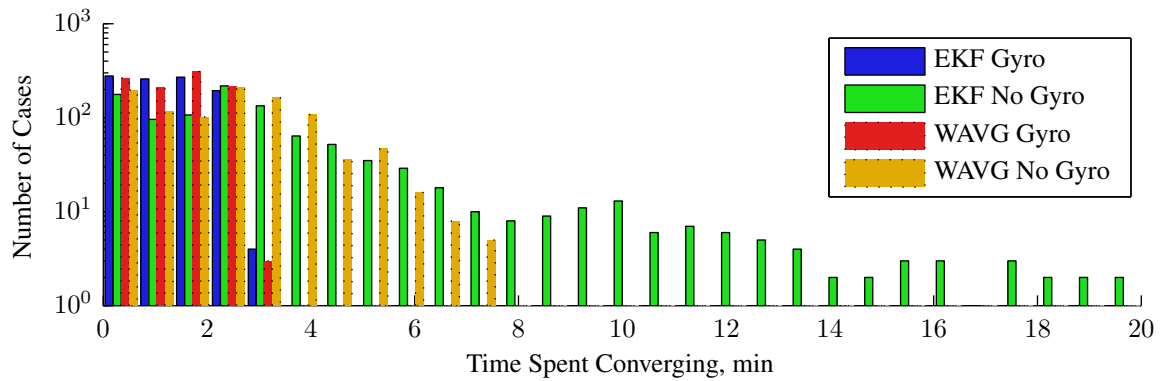
Figure 8: Time spent converging, i.e. solar arrays not pointed within 30 deg of sun vector, for 1000 Monte Carlo simulation cases.

Figure 6, the EKF exhibits better accuracy both with and without angular velocity measurements. Within one orbit the EKF converges to an average error of 2.38 deg with rate measurements and 2.51 deg without rate measurement. The weighted average method converges to an average error of 4.99 deg with and 4.94 deg without rate measurements. The weighted average results correlate well with Figure 2. The average knowledge error seen corresponds to an an attitude error of 10 deg and the 95th percentile knowledge error corresponds to an attitude error of approximately 15 deg which is equal to the controller deadband.

With rate gyroscope measurements both methods can be seen to drive the spacecraft's actual angular velocity and its knowledge of the angular velocity to the noise level. In both cases the angular velocity used in the filter is passed through a 0.1 Hz low pass filter. This filtering is the reason the angular velocity takes time to drop to the noise level. This filter frequency has been selected to reduce the noise in the signal without exciting any unmodeled structural modes.

Without angular velocity measurements both estimate techniques perform similarly well, in conjunction with the controller, bringing the vehicle's angular rates to zero. After 50 minutes the EKF has reduced the average total vehicle angular velocity to 0.67 deg/sec and the weighted average has reduced the total rates to 0.63 deg/sec. The spacecraft's knowledge of its angular velocity is also similar with a value of 0.66 deg/sec for the weighted average method and 0.76 deg/sec for the EKF method.

Of more practical importance is how fast the algorithms in question can reorient the spacecraft to a power positive orientation. It is important to note that the spacecraft is estimating the sun direction vector and controlling its attitude based on that estimation at the same time from the start of the simulation; the control does not wait for estimator convergence to act. Also, in a single orbit the spacecraft may be required to reorient up to two times: the first time the spacecraft senses the sun and when coming out from behind the shadow of Earth. While all cases converged to a power positive orientation, some took longer than others. The total time spent converging, i.e. the amount of time the solar arrays were not pointed within 30 deg of the sun, for each of the four cases is shown in Figure 8.

Both the EKF and the weighted average method show similar performance when angular velocity measurements are available spending less than 3 minutes converging. Significantly more variation is seen between the two methods when no angular velocity measurements are used. In these cases

the larger error in angular velocity of the spacecraft can lead to slow tumbling when in the shadow of the Earth that must be corrected once CSS measurements are available again. The weighted average method spent at most 7.5 minutes converging while the EKF took up to 20 minutes. This time difference is due to the convergence of the EKF. Because the spacecraft control is continuously actuating on the current estimate of the sun direction vector any initial error in that estimate can drive the spacecraft in the wrong direction. However, as the EKF accumulates enough measurements it successfully converges and drives the sun pointing error to zero.

CONCLUSIONS

Two methods for estimating a spacecraft's orientation relative to the Sun using only minimal coarse sun sensors are presented. The first method uses a simple weighted average calculation while the second incorporates an extended Kalman filter. The estimation methods are used in conjunction with a nonlinear three-axis controller to point the spacecraft's solar arrays at the Sun. Both the weighted average and extended Kalman filter formulations are shown to be capable of successfully reorienting a spacecraft from any initial orientation in a reasonable time frame despite the presence of measurement noise.

The weighted average method is attractive because it is computationally simple and insensitive to CSS calibration errors that are common across all sensors, but it provides a less accurate sun direction estimate. The EKF method is attractive as it provides a more accurate estimate of the sun direction vector and utilizes more information to create a more robust estimate, but takes longer to converge when lacking angular velocity measurements. Future research will have to evaluate what impact CSS calibration errors and sensor failures have on both estimator's performance. Even without rate information both methods are capable of bringing the spacecraft to a power positive orientation in a timescale much less than one full orbit thus providing a low cost, low power, coarse sun sensor only solution to reorienting a spacecraft following deployment.

REFERENCES

[1] G. Rufino, M. Grassi, and M. Rolfi, "Preliminary Calibration Results For a High-Precision CMOS Sun Sensor," *AIAA Guidance, Navigation, and Control Conference and Exhibit*, No. August 2008, Honolulu, HI, Aug. 2011, pp. 1–9.

[2] K. Ninomiya, Y. Ogawara, K. Tsuno, and S. Akabane, "High Accuracy Sun Sensor Using CCDs," *AIAA Guidance, Navigation, and Control Conference*, Minneapolis, MN, American Institute of Aeronautics and Astronautics, 1988.

[3] H. D. Black, "A Passive System for Determing the Attitude of a Satellite," *AIAA Journal*, Vol. 2, No. 7, 1964, pp. 1350–1351.

[4] P. B. Davenport, "A Vector Approach to the Algebra of Rotations with Applications," Tech. Rep. August, National Aeronautics and Space Adminstration, Goddard Space Flight Center, Greenbelt, MD, 1968.

[5] M. D. Shuster and S. D. Oh, "Three-Axis Attitude Determination from Vector Observations," *Journal of Guidance, Control, and Dynamics Control and Dynamics*, Vol. 4, No. 1, 1981, pp. 70–77.

[6] F. L. Markley, "Attitude Determination Using Vector Observations: A Fast Optimal Matrix Algorithm," *Journal of the Astronautical Sciences*, Vol. 41, No. 2, 1993, pp. 261–280.

[7] D. Mortari, F. L. Markley, and P. Singla, "Optimal Linear Attitude Estimator," *Journal of Guidance, Control, and Dynamics*, Vol. 30, Nov. 2007, pp. 1619–1627, doi:10.2514/1.29568.

[8] P. Appel, "Attitude Estimation from Magnetometer and Earth-Albedo-Corrected Coarse Sun Sensor Measurements," *Acta Astronautica*, Vol. 56, Jan. 2005, pp. 2–5.

[9] H. Jung and M. L. Psiaki, "Tests of Magnetometer/Sun-Sensor Orbit Determination Using Flight Data," *AIAA Guidance, Navigation, and Control Conference and Exhibit*, No. August, Montreal, Canada, American Institute of Aeronautics and Astronautics, Aug. 2001.

[10] R. E. Kalman, "A New Approach to Linear Filtering and Prediction Problems," *Journal of Basic Engineering*, Vol. 82, No. Series D, 1960, pp. 35–45.

[11] S. Julier, J. Uhlmann, and H. Durrant-Whyte, "A New Approach for Filtering Nonlinear Systems," *Proceedings of 1995 American Control Conference - ACC'95*, Vol. 3, No. 3, 1995, pp. 1628–1632, doi:10.1109/ACC.1995.529783.

[12] B. Jackson and B. Carpenter, "Optimal Placement of Spacecraft Sun Sensors Using Stochastic Optimization," *IEEE Aerospace Conference*, Big Sky, MT, IEEE, Mar. 2004, pp. 3916–3923.

[13] G. M. Lerner, *Spacecraft Attitude Determination and Control*, ch. Sun Sensors, pp. 155–166. Dordrecht, The Netherlands: D. Reidel Publishing Co., 1978.

[14] J. L. Crassidis and J. L. Junkins, *Optimal Estimation of Dynamic Systems*. Applied Mathematics & Nonlinear Science, Chapman and Hall/CRC, 2004.

[15] C. Acton, "Ancillary Data Services of NASA's Navigation and Ancillary Information Facility," *Planetary and Space Science*, Vol. 44, No. 1, 1996, pp. 65–70.

[16] T. W. Flatley and W. A. Moore, "An Earth Albedo Model: A Mathematical Model for the Radiant Energy Input to an Orbiting Spacecraft Due to the Diffuse Reflectance of Solar Radiation From the Earth Below," tech. rep., National Aeronautics and Space Administration, Goddard Space Flight Center, Greenbelt, MD, 1994.

[17] E. A. Hogan and H. Schaub, "Three-Axis Attitude Control using Redundant Reaction Wheels with Continuous Momentum Dumping," *AAS/AIAA Spaceflight Mechanics Meeting*, Kauai, HI, American Institute of Aeronautics and Astronautics, Feb. 2013.